Mid-infrared tunable, narrow-linewidth difference-frequency laser based on orientation-patterned gallium phosphide

Mid-infrared tunable, narrow-linewidth difference-frequency laser based on orientation-patterned gallium phosphide

G Insero[1,2], C Clivati[3], D D'Ambrosio[3], P De Natale[1,2], G Santambrogio[1,2,3], P G Schunemann[4], S Borri[1,2], and J J Zondy[5]

[1]Istituto Nazionale di Ottica, INO-CNR, and European Laboratory for Nonlinear Spectroscopy, LENS, via N. Carrara 1, 50019 Sesto Fiorentino, Italy
[2]Istituto Nazionale di Fisica Nucleare, INFN, Sezione di Firenze, via G. Sansone 1, 50019 Sesto Fiorentino, FI, Italy
[3]Istituto Nazionale di Ricerca Metrologica, INRIM, Strada delle Cacce 91, 10135 Torino, Italy
[4]BAE Systems, Inc., MER15-1813, P.O. Box 868, Nashua, NH, USA 03061-0868
[5]Nazarbaev University, School of Science and Technology, Physics Department, Kabanbay Batyr 53, 010000 Astana, Kazakhstan

E-mail: jeanjacques.zondy@nu.edu.kz

Abstract. We report on the first characterization of orientation-patterned gallium phosphide (OP-GaP) crystals used to generate narrow-linewidth, coherent mid-infrared (MIR) radiation at 5.85μm by difference frequency generation (DFG) of continuous-wave (cw) Nd:YAG laser at 1064nm and diode-laser at 1301nm. By comparison of the experimental absolute MIR efficiency versus focusing to Gaussian beam DFG theory, we derive an effective nonlinear coefficient $d = (1/2)\chi_{eff}^{(2)}$ =17(3) pm/V for first-order quasi-phase-matched OP-GaP at the generated DFG wavelength. Using $d = (2/\pi)d_{14}$ and taking into account Miller's delta rule, we retrieve an absolute value of the d_{14} quadratic nonlinear susceptibility coefficient of GaP of $d_{14} = 27.2(3)$ pm/V at 5.85 μm, in good agreement with the latest absolute measurement of this nonlinear coefficient from non-phase-matched second-harmonic generation (1.32 μm ⟶ 0.66 μm) taking into account multiple reflection effects [Shoji *et al* 1997 *J. Opt. Soc. Am.* B **14** 2268]. The temperature and signal-wave tuning curves are also in qualitative agreement with a recently proposed temperature-dependent Sellmeier equation for OP-GaP when focusing effects are taken into account.

1. Introduction

Narrow-linewidth (<100 kHz), single-frequency and powerful laser sources are needed for precision molecular spectroscopy in the mid-IR range above 5 μm. The 6-μm range is particularly interesting for high-precision spectroscopy of cold CO molecules [1], and the only available sources, with linewidths in the few MHz to tens of MHz range and ~ 0.1W maximum power, are quantum cascade lasers (QCL's) [2]. For precision spectroscopy, μW-level of narrow-linewidth coherent radiation must be produced to either phase-lock or injection-lock such QCL lasers [3, 4].

Continuous-wave (cw) OPOs would be interesting alternative coherent sources combining single-frequency and powerful emission, however except with silver gallium sulfide ($AgGaS_2$) at 2.5 μm [5, 6], genuinely cw mid-IR OPO's have not yet been demonstrated with the existing mid-IR birefringent nonlinear materials (among which $AgGaS_2$, $LiInSe_2$, $CdSiP_2$ [7]) due to their larger residual absorption loss compared to oxide materials ($LiNbO_3$, $KTiOPO_4$ …) whose mid-IR transparency range cut-off

however lies at ~ 4.5 μm. Deeper (> 5 μm) mid-infrared alternatives to oxide quasi-phase-matched (QPM) nonlinear crystals (PPLN, PPLT,…) have appeared since a couple of decade [8], in the form of orientation-patterned III-V semiconductors such as gallium arsenide (OP-GaAs) for which periodical domain inversion is realized during the growth process using molecular beam epitaxy and hydride vapor phase epitaxy (MBE-HVPE) for the re-growth of thicker (~ mm) samples [9, 10]). OP-GaAs cannot be pumped at the popular laser wavelength of 1064nm due to its strong absorption and low energy bandgap. Despite a lower nonlinearity, OP-GaP exhibits a larger bandgap [11] and thus should tolerate 1-μm cw laser pumping, making it a potential candidate for cw OPO emitting above 5 mm. To date however none of them have yet demonstrated *genuinely* cw parametric oscillation. Only *quasi*-cw parametric oscillation at 4.7 μm has been reported for OP-GaAs by chopping the cw pump laser so has to avoid deleterious thermal effects, despite a pump wavelength of 2.1 μm (Ho:YAG laser) where residual absorption is much lower than at 1064 nm [12].

The remaining alternative to cover the 5 – 6 μm range with μW to mW power range from convenient ~1 μm lasers is then to use difference frequency generation (DFG) with a ~ 1.3 μm diode laser in a high-nonlinearity mid-IR crystal. For cw DFG quasi-phase-matched OP-GaAs or OP-GaP are preferable to birefringence phased-matched chalcogenides because the first ones are free from spatial walkoff which dramatically reduces the nonlinear interaction length. While down-conversion schemes using OP-GaAs has been extensively investigated, mostly in the pulsed regime [13,14], to date still few work has been devoted to the newly developed orientation-patterned gallium phosphide (OP-GaP) [15]. A recent cw DFG experiment making use of OP-GaAs pumped by a 40 W Tm: fiber laser at 2.01 μm and a tunable (2.4 – 2.9 μm) cw OPO idler-wave laser with up to 3 W power has yielded multi-tens of mW of 6.4 – 7.6 μm radiation [16]. In the present case where the target MIR range is 5.8 – 6 μm, and given the much lower of the signal-wave diode laser at ~ 1.3 μm, the choice of OP-GaP rather than OP-GaAs is, in addition to its larger thermal conductivity, dictated by its larger bandgap energy which is better suited for a pumping at 1064nm [7].

In this Letter, we provide the first characterization of the linear, thermo-optic and nonlinear properties of OP-GaP via cw DFG of a single-frequency Nd:YAG laser (λ_p = 1064nm, *Mephisto* MOPA, Coherent Inc, linewidth $\Delta\nu$ ~ 10kHz, maximum power 50W) and an extended-cavity tunable diode laser, called here after the signal laser (λ_s = 1301.1nm, DL 100, Toptica Photonics AG, $\Delta\nu \approx$100kHz, maximum power 50 mW). Up to 65 μW of single-frequency idler at λ_i = 5.85 μm have been generated from ~10W of Nd:YAG laser and ~ 45mW of diode laser in a 24.6mm long QPM structure, limited by thermal dephasing effects arising from the non-negligible absorption at the pump and signal lasers' wavelengths, despite the larger bandgap of GaP. From the absolute measurement of DFG conversion efficiency versus focusing and comparison with cw Gaussian beam DFG theory [17] an effective first-order QPM nonlinear coefficient $d = (2/\pi)d_{14}$ =17pm/V (±15%) has been evaluated. From the experimental spectral and temperature tuning curve bandwidths, we could also validate a recently proposed temperature-dependent Sellmeier equation for GaP [15]. Additionally, we have highlighted an OP-GaP/GaAs QPM layer thickness limitation in tightly focused down-conversion processes yielding long-wavelength idler: a minimum QPM layer thickness of $\gtrsim$ 1 mm is required so as to prevent severe loss of the highly diffracting long-wave idler as soon as it expands outside of the periodically-poled layer, due partly to the higher absorption in the (unpoled) bulk semiconductor substrate.

2. DFG experimental setup

In this section we describe the experimental laser set up, the samples of OP-GaAs used and experimental methods aimed at retrieving the absolute value of the effective nonlinear coefficient of OP-GaP.

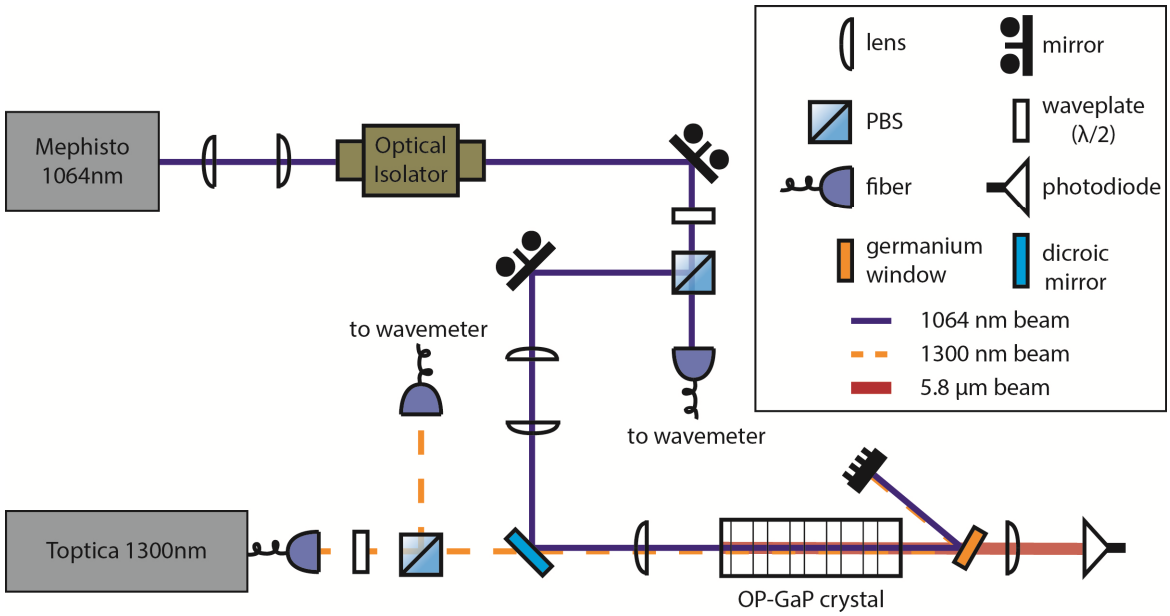

Figure 1. Experimental DFG laser setup. The external-cavity diode laser is fiber-outcoupled. The pump and signal waves are polarized vertically (along the [001] crystallographic axis) and horizontally (along [110]), which yielded horizontally polarized idler radiation. The CaF_2 collecting lens after the Ge filter is actually made of one f = 5 cm lens collimating the diverging idler at the output of the crystal and a second one focusing it on the thermo-electrically cooled 200 μm diameter active area MCT photovoltaic detector. The OP-GaP crystal is hosted in a temperature- regulated oven.

2.1. The laser setup

The layout of the single-pass difference-frequency laser setup is shown in figure 1. The pump laser (*Mephisto* MOPA) is a high-power master-oscillator power-amplifier Nd:YAG laser. The master oscillator is made of a non-planar ring oscillator (NPRO) monolithic cavity, conferring to the emission a narrow short-term linewidth ($\Delta\nu$ = 10 kHz). It injection-locks a subsequent Nd:YAG solid-state power amplifier, capable of delivering up to 50 W of laser power. The *Mephisto* MOPA pump laser output power was however limited to $P_p < 10$ W during the experiment, due to strong absorption of the samples at 1064 nm and thermal saturation of the DFG efficiency. The signal-wave laser (DL 100 Toptica) is a grating-tuned external-cavity diode laser emitting at ~1301 nm. Its output power is limited to 40 mW, so that the pump drive exceeds by far the signal drive. Both near-IR laser beam transverse mode profiles are nearly TEM_{00}.

A variable telescope allows to match the pump beam diameter to the signal beam diameter (D ~ 2mm), and to longitudinally superimpose the two waits inside the crystal during the idler power optimization. The pump and signal beams are superimposed by a dichroic beam-splitter and then focused inside the crystal by several glass (BK7) lenses with various focal lengths (f=150, 100, 75, 50 mm) in order to investigate the dependence of the DFG efficiency on focusing. For tightly focused cw DFG, it is essential to insure a perfect spatial overlap of the two input waists. The common location of the two waists inside the crystal is achieved by fine longitudinal translation of the first telescope lens, while lateral overlap is achieved with slight angular tilts of the beamsplitter (for the pump) and of another (not shown in figure 1) signal laser steering mirror. These fine adjustments are facilitated once enough idler beam signal is detected by the thermo-electrically-cooled mercury cadmium telluride (MCT) photo-voltaic detector equipped with a trans-impedance pre-amplifier (VIGO System). To facilitate idler wave voltage optimization on the oscilloscope monitor, the signal laser is mechanically chopped during the alignments. The generated idler beam at λ_i ~ 5.85 μm is filtered from

the near-IR pump and signal beams using a thick Ge window. The photodetector absolute power responsivity in V/W was calibrated with tens of microwatt radiation form a 6-μm attenuated QCL light that was simultaneously measured by a calibrated powermeter and an absolute radiometer (both giving a consistent power reading to ±5%). All the MIR power reported further has been corrected for all the propagation loss from the OP-Gas output to the MCT detector.

2.2. The OP-GaP samples

The OP-GaP QPM structure was grown by polar-on-nonpolar molecular beam epitaxy (MBE), lithographically patterned, reactive ion-etched and regrown by MBE to yield tens of nanometer-thick templates for subsequent re-growth by low-pressure hydride vapor phase epitaxy (HVPE) [11,15]. The crystal samples carried a 400μm-thick bulk GaP substrate, over which the patterned QPM layer extends for another 400μm thickness. An unpatterned GaP layer extends further above the QPM layer, as a result of the termination of the HVPE regrowth process after the domain walls have coalesced. The duty-cycle quality of the domain period is quite good, showing excellent domain propagation as shown in ref.[15]. The overall thickness of the chips is ~1.5mm, with a ~ 6mm wide QPM layer carrying a 50%-duty cycle periodic domain reversal (grating period $\Lambda = 24\mu m$).

In this experiment, we have used two OP-GaP samples (l_c = 15.3 and 24.6 mm) cut from the $\Lambda = 24$ μm channel. Only the base of the crystals (corresponding to the original wafer base) is optically polished, their upper surface being left rough. Their input/output facets are anti-reflection-coated at the 3 wavelengths ($R_{p,s,i}$ <1%). The overall thickness of the chips is ~1.5mm, with a ~ 6mm wide QPM layer carrying a 50%-duty cycle periodic domain reversal (grating period $\Lambda = 24\mu m$).

The expected quasi-phase-matching temperature for the downconversion process 1064.3 nm – 1301 nm ⟶ 5.85 μm, calculated from the OP-Gas temperature Sellmeier equation [15] is $T \sim 43^o$ C. Therefore, the samples were housed in a massive copper-block oven whose temperature was regulated by a P-I servo-controller, and the oven was mounted on a *XYZ*-θφ positioner for DFG efficiency optimization. No crystal clamping to the polished copper base plate was used, relying on the sole flatness of the polished crystal base to insure thermal conduction (the top groovy facet of the samples did not touch the oven cap, preventing thus heat removal by conduction from this facet). The experimental phase-matching temperature was found to be around $T = 43^o$C as expected. One disadvantage of oven-heating as compared to the use of a thermos-electrically-cooled Peltier element is that while heating process is fast, cooling down the crystal in order to compensate for the thermally-induced radial phase mismatch $\Delta k(T,r)$ arising from the strong pump absorption. Typically we estimate the on-axis ($r = 0$) temperature gradient due to absorption heating to be as large as $\Delta T = 4 – 5^o$C at a pump power of ~ 6–7 W. Each time the pump is ramped, one has to lower gradually the oven set-point temperature in order to optimize the DFG efficiency by partly compensating for the thermally-induced phase-mismatch. For the largest pump power used (P_p = 8–10 W) the oven temperature could no more be decreased below $T \sim 35\text{-}36^o$C due to the thermal inertia of the massive copper block. In future experiments, a thermo-electric cooling method in better suited for the dynamic phase-matching control of the thermally-loaded sample.

Prior to the DFG experiment, the absorption of the OP-GaP chips at both the pump and signal laser wavelengths were cautiously characterized, as the retrieval of the absolute nonlinear coefficient from Gaussian beam DFG theory requires the knowledge of the absorption loss at the near-IR wavelengths (the loss at 6 μm measured from additional FTIR absorption spectrum data is $\alpha_i \sim 0.01$ cm^{-1}). The near-IR loss within the QPM layer was found somewhat less than the absorption loss in the bulk GaP substrate (the HVPE growth technique is almost free from the point defects found in bulk Czochralski-technique growth process). Because the absorption coefficients in the near-IR range as measured by FTIR spectroscopy are less accurate, the absorption coefficient of the samples was measured using the laser sources, by measuring the power transmittance $P_{out}/P_{in} = \exp(-\alpha l_c)$ of the focused laser beams. While inside the 400 μm-thick QPM layer, average measured absorption coefficients amounted to $\alpha_p \approx 0.17$ cm^{-1} and $\alpha_s \approx 0.12$ cm^{-1}, much larger coefficients were found within the bulk substrate (α_p

$\approx 0.58\text{cm}^{-1}$ and $\alpha_s \approx 0.53\text{cm}^{-1}$). Such amount of absorption at 1.3 μm and 1.064 μm within the QPM layer does actually not reflect the intrinsic expected absorption coefficient, which should be much lower according to the larger UV bandgap of GaP compared with GaAs. Further investigation to understand the origin of these absorption bands are being carried out.

2.3. Experimental methods: Waist measurements

In order to analyze the DFG conversion efficiency using Gaussian beam theory [17], it is important to measure as accurately as possible the pump and signal laser waists. The waists $w_{p,s}$ were accurately measured using either the knife-edge technique or the calibrated pinhole transmission technique [19], and were found, as expected for Gaussian beams with equal diameter focused by the same lens, to satisfy the diffraction-limited formula $w = (4/\pi)\lambda f/D$ where f is focal length of the common focusing lens located in front of the sample. As a consequence, all waist ratios were further found to satisfy $w_s/w_p \approx \lambda_s/\lambda_p$. Table 1 summarizes the result of the waist measurements corresponding to the different focusing lenses used. The focused beam DFG theory states that optimal conversion efficiency $\Gamma = P_i/P_pP_s$ (in unit of W/W^2) is achieved when the equal pump/signal confocal parameter condition (ECP) is achieved [17], that is when the two *internal* Rayleigh range $z_{p,s} = \frac{1}{2}k_{p,s}w_{p,s}^2$ are equal ($k = 2\pi n/\lambda$ is the internal wavevector accounting for the index of refraction $n = n(\lambda)$). Although our waist ratio $w_s/w_p \approx \lambda_s/\lambda_p$ does not correspond to the ECP condition ($z_p = z_s$), the experimental ratio is sufficiently close to it. In calculating the theoretical efficiency $\Gamma(w_p, w_s)$ versus the focusing parameter $l = l_c/z_d$, the experimental waist ratio condition must be imposed to confront theory and experimental result. In the definition of the focusing parameter $l = l_c/z_d$, $z_d = \frac{1}{2}k_i w_d^2$ and $w_d = w_p w_s/[w_p^2 + w_s^2]^{1/2}$ are respectively the idler Rayleigh range and idler effective waist (which is smaller than either the pump or signal waist, meaning that the generated idler is highly diffracting all the more than the generated MIR wavelength is long).

Table 1. Measured experimental waists w_p and w_s (±10% uncertainty) and calculated idler waist $w_d = w_p w_s/[w_p^2 + w_s^2]^{1/2}$ and idler Rayleigh range $z_d = (1/2)k_i w_d^2$

f(mm)	w_p (μm)	w_s (μm)	w_d (μm)	z_d (mm)
150	67.5	82.5	52.24	4.67
100	45	55	34.83	2.07
75	27	33	20.90	0.75
50	19	23	14.65	0.37

Among the input beams, the signal wave diffracts more than the pump due to its longer wavelength. However, with the waist values given in table 1, all near-IR input beam modes remains confined with the QPM layer thickness t = 400 μm. For instance, for the strongest focusing conditions (with f = 50 mm) corresponding to a pump and signal confocal parameters $b_p = 2z_p$ = 6.4 mm and $b_s = 2z_s$ = 7.7 mm the pump/signal mode diameters at the exit crystal facet (assuming a waist located at the center of the chip) are not clipped by the QPM layer aperture. However, for the two strongest focusing cases (f = 50 and 75 mm) the output diameter of the generated idler mode that strongly diffracts as it propagates to the output chip facet can be as large as twice the thickness of the QPM layer, meaning that part of the idler mode will experience some additional severe absorption loss from the bulk substrate. Furthermore, for the idler mode volume located outside the QPM layer the QPM condition $\Delta k = 2\pi[n_p - n_s - n_i - 1/\Lambda] = 0$ [8] is no longer satisfied. This propagation of part of the idler energy outside the QPM layer volume may also alter the phase coherence of the DFG process, leading to imperfect constructive interference of each idler wavelet generated in consecutive slabs of the nonlinear material (for downconversion $\varphi_p - \varphi_s - \varphi_i$ depends on the residual phase-mismatch

$\Delta k l_c/2$ which is ~ 0 only within the QPM layer). Indeed we shall observe a drastic reduction of the DFG efficiency for these tightly focused conditions in section 3.

3. Experimental results for DFG conversion efficiencies

Figure 2 displays the absolute MIR power generated by the longest sample (l_c = 24.6 mm) as function of the pump power measured in front of the OP-GaP sample, for a fixed signal wave power P_s ~ 40mW. A similar plot was obtained from the shorter sample. The displayed power has been corrected for all spurious loss in the collecting optics (Ge filter and CaF_2 collecting lenses). Each curve corresponds to the focusing conditions summarized in Table 1. For each data point, the temperature of the oven has been slightly optimized (decreased) as the pump power is ramped so as to partly cancel the thermally-induced phase mismatch. The maximum idler power P_i ~ 65 μW is generated at P_p ~ 10 W at the strongest focusing (f = 50 mm) although the curve for f =75 mm almost overlaps the f = 50 mm curve, meaning that these focal lengths must be around the optimum focusing condition to saturate the DFG efficiency.

The limited transparency of GaP at 1064 nm results in heating of the crystal; the thermo-optic effect consequently changes the refractive index, affecting the QPM conditions. The latter is then responsible for two observed effects. First, at the largest powers, the pump beam heats the crystal by several degrees above the oven copper base temperature, shifting the crystal temperature out of the QPM condition. In our measurements we took into account this shift by decreasing the oven temperature, so that each data point in Figure 2 corresponds to the nearly optimal QPM condition, once thermal equilibrium is reached. Second, the finite thermal conductivity of GaP yields a transverse temperature gradient. This affects the QPM condition in a radially-dependent fashion. While the QPM condition is well satisfied for weak pump powers, for substantial thermal load it cannot be satisfied throughout the whole transverse beams volume. This accounts for the observed idler power saturation at larger pump powers, whereas a linear behaviour would be expected. For the largest pump power (P_p > 6–7 W) it was no longer possible to decrease the oven temperature below T ~ 32°C because of its thermal inertia and the absence of an active cooling mechanism.

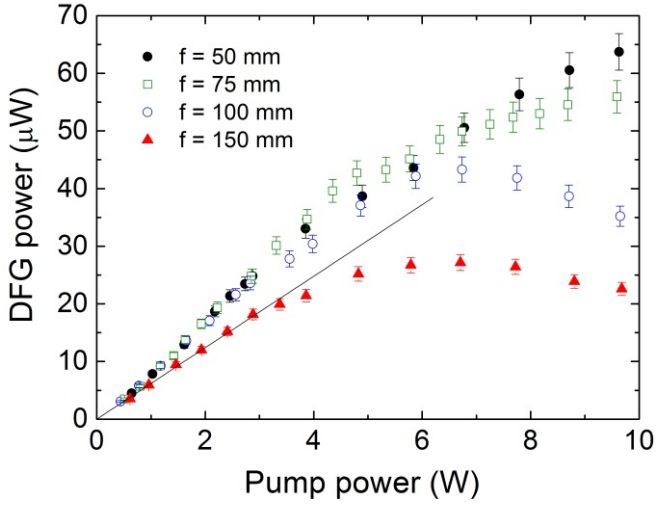

Figure 2. Idler power at λ_i = 5.85 μm versus 1064 nm pump power at maximum ~ 40 mW signal power at 1301 nm.

A striking feature in figure 2 also regards the earlier onset of saturation for loose rather than for strong focusing, while intuitively one would have expected the opposite. The explanation has to do with the poor thermal management (cooling or heating flux occurs through the crystal base only, the upper groovy chip facet not being in contact with the copper cover) and to the relatively large full

transverse diameter ~ 4 w_p of the pump beam respective to the thin QPM layer thickness. For the f = 150 mm data in figure 2 for instance corresponding to cylindrical plane-wave focusing (pump confocal parameter $b_p = 2z_p = 85.6$ mm >> l_c), the on-axis part of the cylindrical Gaussian beam along which the power density is largest cannot be cooled efficiently (the radial extent of the temperature gradient $\Delta T(r)$ is more pronounced for larger transverse beam diameter). By moving vertically the sample position so as to bring the pumped volume toward the colder oven base, beam aperture effect by the thin QPM layer occurs. For stronger focusing instead (e.g. f = 50 and 75mm) the pumped volume in the vicinity of the smaller wait can be moved closer to the oven base which is colder, allowing for a more efficient cooling process by conduction. The same striking feature was also observed for the shorter (l_c=15.3 mm) crystal.

Finally the straight line overriding the loosest focusing data in figure 2 is a fit of the initial linear trend of the conversion efficiency, before the occurrence of thermal load effects. Such line slopes provide the thermal-effect-free conversion efficiency $\Gamma = P_i/P_pP_s$ (plotted as symbols in figure 3) that will be used to retrieve the absolute value of the effective nonlinear coefficient of OP-GaP.

4. Gaussian beam DFG conversion efficiency analysis

In order to evaluate the effective nonlinear coefficient d only the linear data slope of each $P_i = \Gamma P_s P_p$ curve in figure 3 was considered to discard any thermal effects from the analysis. The conversion efficiency Γ (in W^{-1}), obtained by dividing the slope with the constant input power of the signal laser, is plotted against the focusing parameter. The experimental data are then compared with results from the Gaussian beam DFG analysis [17] taking into account the effect of absorption and which further goes beyond the ECP assumption (i.e. valid for any values of $w_{p,s}$). The conversion efficiency Γ from focused Gaussian beam DFG theory taking into account the effect of absorption is given by [17]

$$\Gamma = K\exp(-\alpha_i l_c) l_c \left(k_s^{-1} - k_p^{-1}\right)^{-1} h(a, l, f, \sigma) \tag{1}$$

$$h(a, l, f, \sigma) = \frac{\kappa_e}{2l} \iint_{-f}^{l-f} d\tau d\tau' \frac{\exp[-a(\tau + \tau' + 2f) + i\sigma(\tau - \tau')]}{(1 + i\kappa_e \tau')Q(\tau) + (1 - i\kappa_e \tau)Q^*(\tau')} F_\beta(\tau, \tau').$$

In Equation (1), $K = 8\omega_i^2 d^2/\pi\epsilon_0 c^3 n_p n_s n_i$ is the scaling factor proportional to the square of the effective nonlinear coefficient d, and h is the DFG Gaussian beam focusing function (also called *aperture* function) which depends on the focusing parameter $l = l_c/z_d$, on the normalized phase-mismatch parameter $\sigma = \Delta k z_d$, on the normalized input beam foci location $f = \eta l$ measured from input facet (when absorption cannot be neglected, the relative location η moves ahead from mid-crystal position $\eta = 0.5$ to $\eta < 0.5$ at strong focusing) and on the absorption normalized parameter $a = (\alpha_p + \alpha_s - \alpha_i) z_d/2$. The definition of all parameters in the integral definition of h can be found in [17]. Here we just note that the spatial walkoff function $F_\beta(\tau, \tau')$ in the kernel is set to unity in the case of a quasi-phase-matched down-conversion (scaled walkoff angle $\beta = 0$).

For a given value of the focusing parameter l, and given waist location η, the focusing function $h(a, l, f, \sigma)$ must be optimized (maximized) over the phase-mismatch term σ first. Once this optimum $< h(\eta) >_\sigma$ found, η is incremented (decremented) and a new value of $\sigma_{opt}(\eta)$ is sought until the optimal couple $(\eta_{opt}, \sigma_{opt})$ is found, corresponding to the optimal value of h, noted $< h >_l$ for the focusing parameter l. Then l is incremented and the same multi-variable optimization procedure is repeated so as to construct the theoretical curve $\Gamma(l)$ shown in the next section. Such an optimization of the focusing function, performed using an adaptive step-size FORTRAN algorithm code to repetitively compute the double-integral, actually mimics the experimental optimization of the idler power by optimizing experimentally these parameters by using the sample's XYZ-θφ positioner. The computational optimization procedure yields the expected results that for the rather strong pump and signal absorption loss, the optimal waist location shifts ahead of the sample input facet (η_{opt} ~0.4)

instead of being located at mid-sample (η_{opt} = 0.5) for the two strongest focusing cases. Additionally, the retrieved values of σ_{opt} are not nil as it is for plane-wave DFG but have negative non zero values as a result of focusing [17]. In performing the computational optimization leading to the curves $\Gamma(l)$, the experimental condition $w_s/w_p \approx \lambda_s/\lambda_p$ has been imposed. Once $< h(l) >$ is evaluated, the scaling factor K in (1) is then adjusted via d to match the curves to the experimentally determined $\Gamma(l)$'s.

5. Experimental DFG efficiencies and retrieval of the effective nonlinear coefficient

The comparison between experimental Γ's (symbols) and DFG theory (solid lines) is shown in figure 3 for both sample lengths, where the nonlinear effective d was adjusted to the two loose focusing data rather than the strong focusing ones for the reasons stated at the end of subsection 2.3, related to the efficiency limitations arising from the limited QPM layer thickness under strong focusing conditions (the fact that the generated idler mode expands then outside the QPM layer, in the severely absorbing bulk substrate). For those reasons we have chosen to match the theoretical $\Gamma(l)$ curves to the two loose focusing data point only for which all pump, signal *and* idler modes remain confined within the QPM volume. It thus appears that the two strong focusing data tend to depart from the predicted theoretical optimum for both samples, and such a departure is not due to thermal effects since the experimental Γ's are derived from the slope of the low-power linear data in figure 2.

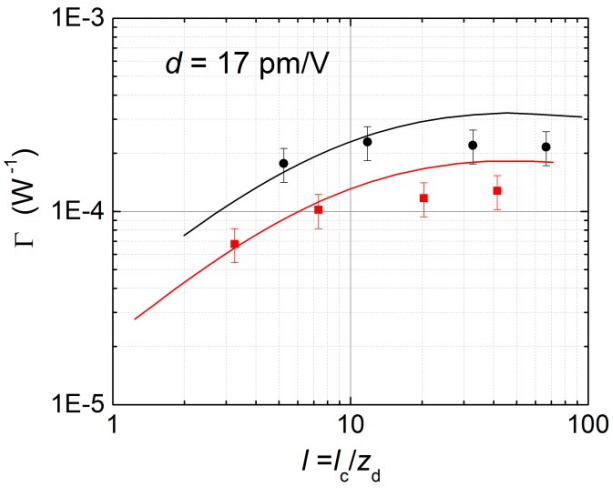

Figure 3. Plot of the absolute DFG conversion efficiency Γ as function of the focusing parameter l (crystal length expressed in units of the idler Rayleigh length). Experimental data are plotted as symbols (squares for the l_c = 15.3 mm OP-GaP sample and circles for l_c = 24.6 mm sample). The solid lines represent the optimized theoretical efficiency.

The best curve match to the loose focusing experimental data is found for d =17(3) pm/V. The ±3 pm/V uncertainty originates from the waist measurement uncertainty and absolute idler power uncertainty. The fact the departure of the two strong focusing data from the predicted optimum focusing is more pronounced for the longer crystal corroborates our assumption that the QPM layer thickness must be increased to ~ 0.8 – 1 mm so as to confine the highly diverging ($\delta = \lambda_i/\pi n_i w_d$) idler wave within the QPM layer volume over the total sample length.

It is interesting to compare the measured absolute effective nonlinear coefficient $d = (2/\pi)d_{14}$ to values of the $d_{14}(\equiv d_{36})$ coefficient of GaP derived from non-phase-matched second-harmonic generation in bulk isotropic GaP. Levine reported $d_{14} = 37(2)$ pm/V from Maker-fringe technique at 10.6 μm (5.3 μm SH), $d_{14} = 49(9)$ and 47(10) pm/V from wedge technique at 1.32 μm (0.63 μm

SH) and 2.12 μm (1.06 μm SH), respectively [20]. More recently, Shoji *et al*. accurately measured $d_{14} = 36.8(4)$ pm/V from wedge technique at 1.32 μm taking for the first time into account multiple reflection effects that may play an important role in the previous measurements given the high index of refraction of GaP ($n \sim 3$ in the mid-IR) [21]. Note that the measurements by Levine have been rescaled to lower values following the standardization recommendation by Roberts [22]. Applying the Miller's rule factor $M_{14} = \prod_{i=1}^{3} (n^2(\lambda_i) - 1)/(n^2(\Lambda_i) - 1)$ to take account of $\chi^{(2)}$ dispersion, where the Λ_i are Shoji's reference second-harmonic generation wavelengths and using a recently determined temperature-dependent Sellmeier equation to account for dispersion [15], one finds $M_{14} = 0.82$ for our DFG wavelengths, and thus a nonlinear coefficient $d_{14} = 30.2$ pm/V for 5.85 μm generation using the present down-conversion pump and signal wavelength, from Shoji's most reliable measurement. For first-order QPM, this yields $d = 19(2)$ pm/V, close to our experimental value $d = 17(3)$ pm/V. Our d value translates into $d_{14} = 27.2(3)$ for GaP at ~ 6 μm.

6. Angular and spectral tuning curves

We have also investigated the temperature and signal wavelength DFG tuning curves, and compared the experimental acceptance curves with the theoretical curve given by $h(\sigma)$ where the wavevector-mismatch parameter $\Delta k(T, \lambda_i)$ in the reduced parameter $\sigma = \Delta k z_d$ has been evaluated with the temperature-dependent Sellmeier equation of Ref. [15] that was derived from the temperature-tuned wavelengths of a nanosecond Nd:YVO_4 pumped OP-GaP mid-IR OPO. Figure 4 compares the experimental and theoretical temperature tuning curve and figure 5 the spectral tuning curve when the Toptica diode laser was tuned around the phase-matched signal wavelength. Both the cylindrical focusing (f = 150mm, black circles) and strong focusing (f = 75mm, hollow circles) cases are plotted, and compared with simple plane-wave prediction ($\propto \mathrm{sinc}^2(\Delta k l_c/2)$, dashed curve) and the Gaussian beam DFG theory prediction (solid curves).

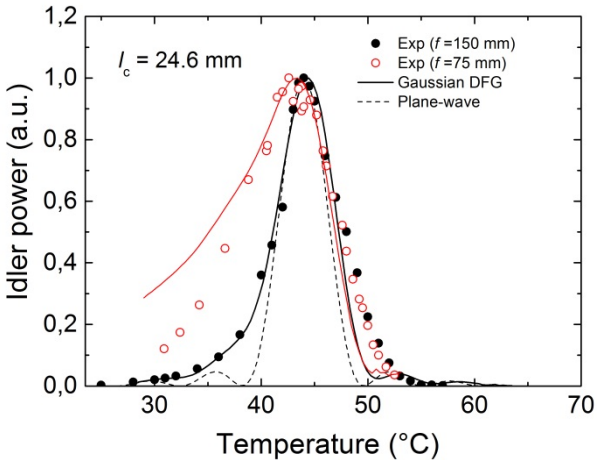

Figure 4. Temperature tuning curves for loose and strong focusing conditions (long sample). The dashed line is a plane-wave pattern.

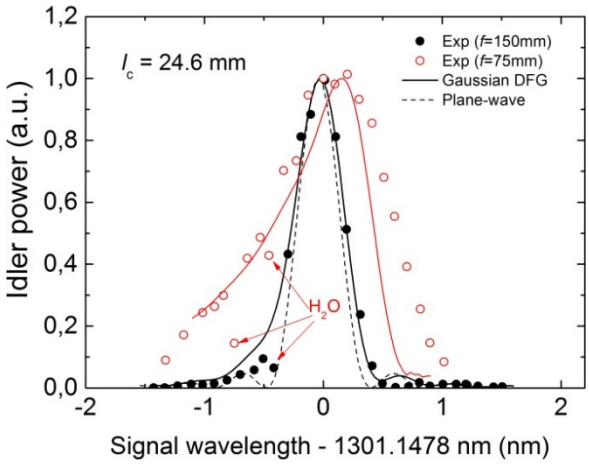

Figure 5. Signal-wave tuning curves for loose and strong focusing conditions. The arrows point to water line absorption as predicted by atmospheric databases near 5.85μm [23].

It can be seen that the broadening and asymmetry of the tuning curves at strong focusing are qualitatively accounted by the focused-beam DFG theory. It can also be noticed that beam aperture effects wash out the usual side lobes of the plane-wave tuning curve. At looser focusing there is a good match between both experiment and theory as to the temperature and spectral acceptance bandwidths, validating thus the thermo-optical dispersion relation given in Ref. [15].

7. Conclusions

In conclusion, we report on the first complete characterization of the cw difference-frequency generation process in an OP-GaP crystal, and demonstrate the first DFG using OP-GaP. The maximum generated idler power of ~ 65 μW is limited by thermal effects arising from the substantial absorption at 1064 nm by the OP-GaP samples. As the absorption coefficients of OP-GaP for wavelengths beyond 1.5 μm are about one order of magnitude lower than at 1064 nm, a pump laser in the telecom band around 1550 nm would allow to increase significantly the idler power (diode lasers for the signal around 2 μm are commercially available). The generated radiation can be referred to an absolute frequency standard by locking the pump and signal lasers to a near-IR comb, and the narrow-linewidth DFG radiation is sufficient to phase-lock a broader-linewidth QCL.

Funding. The ELI European project; Instituto Nazionale di Fisica Nucleare (INFN) (SUPREMO); Horizon 2020 (EMPIR-15SIB05-OFTEN); Participating Sates.

Acknowledgments

EMPIR-15SIB05-OFTEN has received funding from the EMPIR programme co-financed by the Participating States and from the European Union's Horizon 2020 research and innovation programme.

References

[1] Borri S and Santambrogio G *Adv. in Phys*.: X 2016 doi: 10.1080/23746149.2016.1203732
[2] Bartalini S, Borri S, Galli I, Giusfredi G, Mazzotti D, Edamura T, Akikusa N, Yamanishi M. and De Natale P 2011 *Opt. Expr.* **19** 17996
[3] Borri S, Galli I, Cappelli F, Bismuto A, Bartalini S, Cancio P, Giusfredi G, Mazzotti D, Faist J and De Natale P 2012 *Opt. Lett.* **37** 1011
[4] Galli I, Siciliani de Cumis M, Cappelli F, Bartalini S, Mazzotti D, Borri S, Montori A, Akikusa N, Yamanishi M, Giusfredi G, Cancio P and De Natale P 2013 *Appl. Phys. Lett.* **102** 121117
[5] Douillet A and Zondy J J 1998 *Opt. Lett.* **23** 1259
[6] Douillet A, Zondy J J, Yelisseyev A, Lobanov S and Isaenko L 1999 *J. Opt. Soc. Am.* B **16** 1481
[7] Petrov V 2015 *Prog. Quantum Electron.* **42** 1
[8] Hum D S and Fejer M M 2007 *C. R. Physique* **8** 180
[9] Koh S J, Kondo T, Ishiwada T, Iwamoto C, Ichinose H, Yaguchi H, Usami T, Shiraki Y and Ito R 1998 *Jpn. J. Appl. Phys.* **37** L1493
[10] Ebert C B, Eyres L A, Fejer M M and Harris J S 1999 *J. Crystal Growth* **201/202** 187
[11] Tassev V, Snurea M, Petersona R, Scheplera K L, Bedforda R, Manna M, Vangalab S, Goodhuec W, Lind A, Harris J, Fejer M and Schunemann P 2013 *Proc. SPIE* **8604** 86040V
[12] Pomeranz L, Schunemann P, Setzler S, Jones C and Budni P 2012 *CLEO-OSA Technical Digest*, paper JTh1I.4 doi:10.1364/CLEO_AT.2012.JTh1I.4
[13] Hildenbrand A, Kieleck C, Lallier E, Faye D, Grisard A, Gérard B and Eichhorn M 2011 *Proc. SPIE* **8187** 81870H
[14] Leindecker N, Marandi A, Byer R L, Vodopyanov K L, Jiang J, Hartl I, Fermann M and Schunemann P G 2012 *Opt. Express* **20** 7047
[15] Pomeranz L A, Schunemann P G, Magarrell D J, McCarthy J C, Zawilski K T and Zelmon D E 2015 *Proc. SPIE* **9347** 93470K
[16] Devi K, Schunemann P G and Ebrahim-Zadeh M 2014 *Opt. Lett.* **39** 6751
[17] Zondy J J 1998 *Opt. Commun.* **149** 181
[18] P. Kuo, PhD dissertation, http://nlo.stanford.edu/content/thick-film-orientation-patterned-gallium-arsenide-nonlinear-optical-frequency-conversion
[19] Zondy J J, Touahri D and Acef O 1997 *J. Opt. Soc. Am.* B **14** 2481
[20] Levine Z H 1994 *Phys. Rev.* B **49** 4532
[21] Shoji I, Kondo T, Kitamoto A., Shirane M and Ito R 1997 *J. Opt. Soc. Am.* B **14** 2268
[22] Roberts D A 1992 *IEEE J. Quantum Electron*. **28** 2057
[23] HITRAN, http://hitran.iao.ru/